

# Absorbing state dynamics of stochastic gradient descent

Guanming Zhang<sup>1,2</sup> and Stefano Martiniani<sup>1,2,3</sup>

<sup>1</sup>Center for Soft Matter Research, Department of Physics, New York University, New York 10003, USA

<sup>2</sup>Simons Center for Computational Physical Chemistry, Department of Chemistry, New York University, New York 10003, USA\*

<sup>3</sup>Courant Institute of Mathematical Sciences, New York University, New York 10003, USA<sup>†</sup>

Stochastic gradient descent (SGD) is a fundamental tool for training deep neural networks across a variety of tasks. In self-supervised learning, different input categories map to distinct manifolds in the embedded neural state space. Accurate classification is achieved by separating these manifolds during learning, akin to a packing problem. We investigate the dynamics of “neural manifold packing” by employing a minimal model in which SGD is applied to spherical particles in physical space. In this model, SGD minimizes the system’s energy (classification loss) by stochastically reducing overlaps between particles (manifolds). We observe that this process undergoes an absorbing phase transition, prompting us to use the framework of biased random organization (BRO), a nonequilibrium absorbing state model, to describe SGD behavior. We show that BRO dynamics can be approximated by those of particles with linear repulsive interactions under multiplicative anisotropic noise. Thus, for a linear repulsive potential and small kick sizes (learning rates), BRO and SGD become equivalent, converging to the same critical packing fraction  $\phi_c \approx 0.64$ , despite the fundamentally different origins of their noise. This equivalence is further supported by the observation that, like BRO, near the critical point, SGD exhibits behavior consistent with the Manna universality class. Above the critical point, SGD exhibits a bias towards flatter minima of the energy landscape, reinforcing the analogy with loss minimization in neural networks.

Stochastic gradient descent (SGD) is widely used in machine learning and optimization, particularly for training deep neural networks (DNN), due to its efficiency and ability to handle large datasets via batch optimization [1–7]. When training a DNN, the discrepancy between the data and the model’s prediction is given by a loss function [8–13]. SGD iteratively updates the model’s weights by performing gradient descent on randomly selected batches of data to minimize the loss. Despite being overparameterized, DNNs trained with SGD exhibit surprisingly strong generalization performance. While a comprehensive theory of deep learning is still under development [14–20], it is hypothesized that this generalization ability arises from the interplay between training dynamics and the geometric structure of the loss landscape of DNNs [21–23]. Therefore, developing a deeper understanding of SGD dynamics is of critical importance.

In the neural state space, points representing neural responses to inputs from the same class collectively form a distinct manifold (Fig. 1). Classification aims to distinguish these manifolds using a readout network (or decoder). If the finite-sized neural manifolds representing “cats” and “dogs” were to overlap, some dogs would be perceived as cats and vice versa, resulting in decoding errors. As a result, classification can be seen as a packing problem in neural state space. A simplistic alternative would be to shrink each manifold to a single point, eliminating overlaps entirely. However, if the “cats” manifold collapsed to a point, all cats would be perceived as identical, making the representation inadequate for other downstream tasks requiring detailed differentiation.

An example of how deep learning techniques explicitly manipulate the neural state space is self-supervised

learning (SSL). SSL enables models to learn meaningful representations without large labeled datasets. Recent advances show that SSL can match or even outperform supervised learning across various tasks [24–26].

In a simplified theoretical treatment, where neural manifolds are conceptually enclosed within spheres, the training problem reduces to finding configurations where these spheres do not overlap (Fig. 1). In the limit of a large number of classes encoded by the responses of a downstream layer of 3 neurons (i.e., in  $3d$  embedded neural state space), this problem reduces to the classical sphere packing problem studied in physics [27, 28], and, in higher dimensions, to sphere packing problems considered in mathematics and information theory [29].

Manifold capacity theory (MCT) quantifies the capacity of a linear decoder for *binary* classification of neural

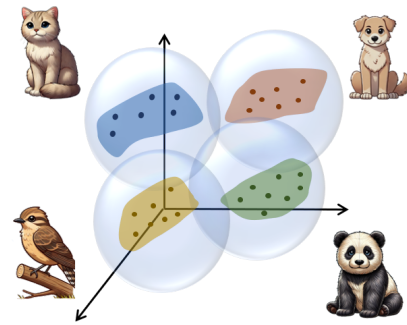


FIG. 1. Neural manifold packing. Each manifold in the embedded neural state space represents an animal class. When the manifolds are enclosed by spheres, the classification problem reduces to a sphere packing problem.

manifolds [30, 31], with recent work extending it to binary classification with nonlinear decoders [32]. Unlike MCT, we focus on the learning dynamics of the encoder for the general  $n$ -ary classification problem (i.e.,  $n \gg 2$ ), which is the relevant setting for SSL, rather than on the binary capacity of the decoder. Our analysis is also different from previous studies that proposed a more tentative link between classification and packings in weight space [10]. Instead, we argue that the connection to neural state space, inspired by contemporary systems neuroscience, is more direct and concrete.

A particularly insightful perspective on the packing problem is offered by random organization. Originally introduced to model the dynamics of driven colloidal suspensions, [33–35] these “absorbing state models” exhibit a nonequilibrium phase transition from an absorbing (inactive) state, where all geometric constraints are satisfied (i.e., no particle overlaps), to an active steady-state with unresolved constraints. The dynamics of random organization models are prescribed by local stochastic rules. For instance, in Biased Random Organization (BRO), the system evolves by randomly displacing overlapping particles away from one another. BRO displays several properties characteristic of random close packing (RCP), such as a critical point at volume fraction  $\phi_c \approx 0.64$ , while also displaying Manna universality scaling [36, 37]. When particle updates in BRO involve nonreciprocal, particle-wise kicks that do not strictly conserve center of mass, we refer to this variant as “particle-wise BRO”. Conversely, if the kicks are reciprocal and the updates conserve center of mass, we denote it as “pairwise BRO”. Recent studies have demonstrated that pairwise BRO exhibits long-range order in  $2d$ , violating the Mermin-Wagner theorem [38], and that density fluctuation in the active phase are anomalously suppressed [39].

The defining features of BRO’s random kicks are their inherent bias – particles repel each other even without an explicitly defined potential – and their sizes, which are determined by a multiplicative noise process, ensuring that kicks are nonzero only when particles overlap. Notably, these properties resemble certain characteristics of SGD [18, 40, 41]. The crucial difference between BRO and SGD lies in the origin of their noise: in BRO, it arises from the variability in kick sizes, whereas in SGD, it results from the randomness of batch selection. Whether these processes share similarities, or can be unified under a common framework, remains an open question – one that we address in this work, demonstrating that such unification is indeed possible.

In this work, we examine the absorbing state dynamics of neural manifold packing through BRO and SGD, specifically in the limit of a large number of classes (particles) within a three-dimensional embedded neural state space. This approach allows us to establish direct connections between our findings and the physics literature on BRO. We begin by showing that the discrete particle-

wise and pairwise BRO dynamics can be effectively approximated by the dynamics of linearly repulsive particles driven by anisotropic multiplicative noise, defined at the single-particle and particle-pair levels, respectively. We then analytically and numerically demonstrate that particle-wise and pairwise SGD for a system of linear-repulsive particles closely approximates particle-wise and pairwise BRO. Across all schemes, BRO and SGD achieve the same critical packing fraction in the limit of zero kick size (or learning rate, for SGD) in three dimensions, coinciding with the random close packing fraction,  $\phi_c \approx 0.64$  [34, 42–46]. In all cases the critical behavior near the critical point is in the Manna universality class. This consistency holds regardless of batch size, even in the zero noise limit of SGD (i.e., gradient descent). These results suggest that the distinctive noise characteristics of the different processes are unimportant near criticality. In contrast, in the active phase at higher packing fractions, pairwise SGD with smaller batch sizes favors flatter minima, whereas particle-wise SGD is biased towards sharper minima.

**Pairwise BRO as linear-repulsive particles driven by anisotropic multiplicative noise.** In the pairwise BRO model, each pair of overlapping particles is displaced by equal-magnitude vectors in opposite directions along the line connecting their centers. The magnitude of these displacements is sampled uniformly from the range  $[0, \epsilon]$ , where  $\epsilon$  denotes the kick size. In each iteration, overlapping particles, which are said to be “active”, are updated, while isolated particles, termed “inactive”, remain unchanged. This process is repeated until the system either reaches an absorbing state with no active particles or attains an active steady state where the fraction of active particles stabilizes around some value  $0 < f_a \leq 1$ . Fig. 2(a) illustrates the dynamics of pairwise BRO (See Supplementary Material for the algorithmic description). The update rule for active particle  $i$  at

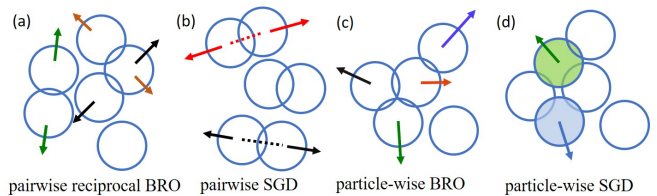


FIG. 2. Schematics of (a) Pairwise reciprocal BRO: each active pair is kicked randomly by opposite equally-sized vectors. (b) Pairwise SGD: two of three active pairs (dashed lines) are selected to form a batch, and gradient descent is performed individually for each pair. (c) Particle-wise BRO: each active particle is randomly kicked away from all overlapping particles. (d) Particle-wise SGD: two of five particles (shaded) are selected to form a batch, and gradient descent is performed for each of the batch particles with respect to all interactions.

iteration  $k$  then reads [36, 47],

$$\mathbf{x}_{k+1}^i = \mathbf{x}_k^i + \epsilon \sum_{j \in \Gamma_k^i} u_k^{ji} \Delta \mathbf{x}_k^{ji}, \quad (1)$$

where  $\mathbf{x}_k^i$  is the position of particle  $i$  at time step  $k$ , and  $\Delta \mathbf{x}_k^{ji} = -(\mathbf{x}_k^j - \mathbf{x}_k^i) / |\mathbf{x}_k^j - \mathbf{x}_k^i|$  is the direction of the kick from particle  $j$  to  $i$ .  $\epsilon$  is the kick size,  $u_k^{ji}$  is a ‘‘reciprocal’’ noise sample drawn uniformly from  $[0, 1]$  such that  $u_k^{ji} = u_k^{ij}$ .  $\Gamma_k^i = \{j \mid |\mathbf{x}_k^j - \mathbf{x}_k^i| < 2R\}$  is the set of all particles overlapping with particle  $i$  at the iteration  $k$ , and  $R$  is the particles’ radius.

To derive a stochastic approximation of these dynamics [17, 48], we decompose the biased random kick on each pair into its mean value,  $\mathbf{g}_k^{ji} = \mathbb{E}[\Delta \mathbf{x}_k^{ji} u_k^{ji}] = \Delta \mathbf{x}_k^{ji} / 2$ , and the fluctuation around the mean,  $\mathbf{z}_k^{ji} = u_k^{ji} \Delta \mathbf{x}_k^{ji} - \mathbf{g}_k^{ji}$ . We then approximate the random fluctuations by a Gaussian random variable,  $\boldsymbol{\eta}_k^{ji} \sim \mathcal{N}(\mathbf{0}, \boldsymbol{\Sigma}^{ji})$ , with covariance  $\boldsymbol{\Sigma}^{ji} = \mathbb{E}[\mathbf{z}_k^{ji} \mathbf{z}_k^{jiT}] = \frac{1}{3} \mathbf{g}_k^{ji} \mathbf{g}_k^{jiT}$ . As a result, Eq. 1 is approximated by the process

$$\mathbf{x}_{k+1}^i = \mathbf{x}_k^i + \epsilon \sum_{j \in \Gamma_k^i} (\mathbf{g}_k^{ji} + \boldsymbol{\eta}_k^{ji}), \quad (2)$$

We note that the  $\mathbf{g}_k^{ji}$  is equivalent to the negative gradient of the pairwise potential energy of short-ranged, linear-repulsive particles,

$$\begin{aligned} \mathbf{g}_k^{ji} &= -\nabla^i U(|\mathbf{x}_k^i - \mathbf{x}_k^j|) \\ \mathbf{U}(\mathbf{r}) &= \begin{cases} \frac{1}{2}(2R - |\mathbf{r}|), & \text{if } |\mathbf{r}| < 2R \\ 0, & \text{otherwise} \end{cases} \end{aligned} \quad (3)$$

Thus, we can define the total potential energy  $V = \sum_i \sum_{j>i} U(|\mathbf{x}_k^i - \mathbf{x}_k^j|)$ , such that  $\nabla^i V = -\sum_j \mathbf{g}_k^{ji}$ , and rewrite Eq. 2 to arrive at the stochastic approximation,

$$\begin{aligned} \mathbf{x}_{k+1}^i &= \mathbf{x}_k^i - \epsilon \nabla^i V + \frac{\epsilon}{\sqrt{3}} \sum_j \sqrt{\boldsymbol{\Lambda}^{ji}} \cdot \boldsymbol{\xi}_k^{ji}, \text{ where} \\ \boldsymbol{\Lambda}^{ji} &= \nabla^i U(|\mathbf{x}_k^i - \mathbf{x}_k^j|) \nabla^i U(|\mathbf{x}_k^i - \mathbf{x}_k^j|)^T \end{aligned} \quad (4)$$

$\boldsymbol{\xi}_k^{ji}$  is standard Gaussian noise modelling the reciprocal, pairwise kick from  $j$  to  $i$ , such that  $\boldsymbol{\xi}_k^{ji} = -\boldsymbol{\xi}_k^{ij} \cdot \sqrt{\boldsymbol{\Lambda}^{ji}}/3$  is the matrix square root of the covariance matrix, which scales and projects the noise along the lines connecting the particles centers. Eq. 4 demonstrates that the BRO dynamics are equivalent to those of linearly repulsive particles driven by anisotropic multiplicative noise.

In the limit of small kick size, the BRO dynamics can be further approximated as a continuous-time process described by the stochastic differential equation [16, 17, 49],

$$d\mathbf{x}^i(t) = -\frac{\epsilon}{\tau} \nabla^i V dt + \frac{\epsilon}{\sqrt{3}\tau} \sum_j \sqrt{\boldsymbol{\Lambda}^{ji}(t)} \cdot d\mathbf{W}^{ji}(t) \quad (5)$$

where  $\mathbf{x}^i(t)$  and  $\boldsymbol{\Lambda}^{ji}(t)$  are the continuous-time counterparts of the discrete-time variables in Eq. 4 and  $\tau$  is the time scale measuring the time elapsed between two discrete steps (see Supplemental Materials).

### Pairwise SGD approximates BRO dynamics.

In the context of interacting particle systems, we introduce *pairwise SGD*, inspired by the SGD method widely used in machine learning. During each iteration  $k$ , an active pair (a pair of particles  $i$  and  $j$  such that  $|\mathbf{x}_k^i - \mathbf{x}_k^j| \leq 2R$ ) is selected with probability  $b_f$ , equal to the fraction of pairs in a batch. Each particle in the selected pair is then moved by equal but opposite displacements  $-\alpha \nabla^i U(|\mathbf{x}_k^i - \mathbf{x}_k^j|)$  and  $-\alpha \nabla^j U(|\mathbf{x}_k^i - \mathbf{x}_k^j|)$ , where  $\alpha$  is the learning rate. We choose the interaction potential  $V = \sum_i \sum_{j>i} U(|\mathbf{x}_k^i - \mathbf{x}_k^j|)$  to be pairwise, short-ranged and linearly-repulsive, as in Eq. 3, to be consistent with the pairwise BRO process. However, the potential energy  $V$  minimized by SGD need not be the same as in Eq. 3, in fact other choices of pairwise potentials (e.g., Lennard-Jones [50], WCA [51], etc.) can be used to construct a valid SGD process.

Selecting a batch of active pairs corresponds to selecting a subset of terms in the sum defining  $V$ , which is a sum over pairwise interactions. This is analogous to selecting a subset of terms from the loss function  $\mathcal{L}(\mathcal{D}) = \sum_{\mathbf{x}_j \in \mathcal{D}} L[f(\mathbf{x}_j), \hat{f}_\theta(\mathbf{x}_j)]$  where  $\mathcal{D} = \{\mathbf{x}_1, \dots, \mathbf{x}_N\}$  is a dataset,  $f(\mathbf{x}_j)$  is the target value, and  $\hat{f}_\theta(\mathbf{x}_j)$  represents the model output, parametrized by  $\theta$ . Selecting a pair of particles is akin to selecting a pair of data samples. If the samples belong to different classes but their corresponding manifolds overlap, they are likely to be misclassified as belonging to the same class. Thus, during training, the manifold centers will move to reduce  $\mathcal{L}$  (via an appropriate change in  $\theta$ ), effectively decreasing the manifold overlap and correcting the classification.

To approximate the stochastic updates in SGD, we determine the probability distribution for selecting a particle pair and then calculate the mean and covariance of the descent step. Following the same stochastic approximation approach used in Eq. 2, we arrive at the following stochastic approximation of the SGD dynamics (see Appendix for details)

$$\mathbf{x}_{k+1}^i = \mathbf{x}_k^i - \alpha b_f \nabla^i V + \alpha \sqrt{b_f - b_f^2} \sum_{j \in \Gamma_k^i} \sqrt{\boldsymbol{\Lambda}^{ji}} \cdot \boldsymbol{\xi}_k^{ji}, \quad (6)$$

where  $\boldsymbol{\xi}_k^{ji}$  is the standard Gaussian noise satisfying reciprocity,  $\boldsymbol{\xi}_k^{ji} = -\boldsymbol{\xi}_k^{ij}$ . The noise term in Eq. 6 has the same functional form as Eq. 4, illustrating the shared stochastic nature for SGD and BRO. If we set  $\alpha = \epsilon/b_f$  and  $b_f = 3/4$ , where  $\epsilon$  is the kick size in the BRO dynamics, then Eq. 6 matches exactly Eq. 4. Again, in the limit of infinitesimal learning rate, the pairwise SGD dynamics approximates the continuous time stochastic differential equation,

$$d\mathbf{x}^i(t) = -\frac{\alpha b_f}{\tau} \nabla^i V dt + \frac{\alpha}{\sqrt{\tau}} \sqrt{b_f - b_f^2} \sum_j \sqrt{\Lambda^{ji}(t)} \cdot d\mathbf{W}^{ji}(t). \quad (7)$$

**Particle-wise SGD approximates particle-wise BRO dynamics.** An alternative implementation of BRO applies particle-wise kicks at each iteration. In this approach, each overlapping neighbor of particle  $i$  contributes a unit kick, and the resultant vector is scaled by a random number drawn from a uniform distribution over  $[0, \epsilon]$ , which then displaces particle  $i$ . We find that such a process approximates particle-wise SGD, where each active particle has probability  $b_f$  to be selected and moved along its gradient by  $-\alpha \nabla^i V$  (see Appendix and Supplementary Material). Specifically, when  $\alpha = \epsilon/b_f$  and  $b_f = 3/4$ , the stochastic approximations for particle-wise BRO and SGD are equivalent.

**Critical behavior of SGD.** We numerically compare the dynamics of BRO, SGD, and their stochastic approximations, finding that in the limit of small kick sizes, their mean square displacements agree, and their critical packing fractions converge,  $\phi_c \rightarrow \phi_{RCP} \approx 0.64$  as  $\epsilon \rightarrow 0$  (or learning rate  $\alpha \rightarrow 0$  for SGD) (Appendix and Supplementary Material).

Thus, it becomes compelling to test whether SGD, like BRO, belongs to the Manna (conserved direct percolation) universality class. We measure the steady state “activity”,  $f_\infty^a$ , and the relaxation time  $\tau_r$ . The activity  $f_k^a$  is defined as the ratio between the number of overlapping particles and the total number of particles at time step  $k$ , and  $\tau_r$  measures the time for the system to reach the steady state. On the absorbing side,  $\phi < \phi_c$ ,  $\tau_r$  is the time required for the system to absorb,  $f_{\tau_r}^a = 0$ . On the active side,  $\phi > \phi_c$ , where the system never reaches an absorbing state and evolves forever, we estimate  $\tau_r$  as the first time that the activity drops to within  $(f_k^a - f_\infty^a)/f_\infty^a < 0.1$  [38]. Random organization models display critical scalings  $f_\infty^a \sim (\phi - \phi_c)^\beta$  and  $\tau_r \sim |\phi - \phi_c|^{-\nu_\parallel}$  in the proximity of  $\phi_c$ , where  $\beta = 0.84$  and  $\nu_\parallel = 1.08$  are the Manna exponents [34, 36, 52, 53].

We test this hypothesis by performing finite size scaling analysis for the activity and relaxation time of SGD at different batch fractions,  $b_f$ , assuming the Manna exponents [54] and fitting  $\phi_c$  using Pyfssa [55], see Fig. 3 (and Supplementary Material). The data collapses are convincing both for pairwise and particle-wise SGD, irrespective of batch fractions ( $b_f$ ), which corresponds to different noise levels. When  $b_f = 1.0$ , both particle-wise and pairwise SGD reduce to gradient descent (GD), corresponding to the zero noise limit of SGD. Consequently, the critical behavior for SGD and GD are consistent with the Manna universality class. However, it is important to note that GD is not an absorbing state model, as it “absorbs” on both sides of  $\phi_c$ . For  $\phi > \phi_c$ , GD settles into an overlapping state (a minimum of the potential  $V$ )

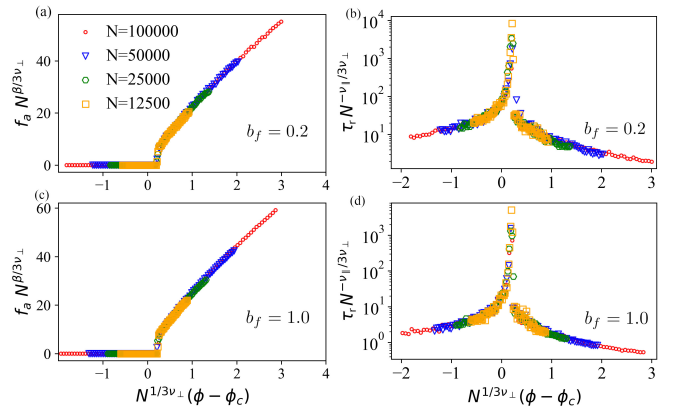


FIG. 3. Finite size scaling analysis for pairwise SGD: Steady-state activity as a function of packing fraction,  $\phi$ , for (a)  $b_f = 0.2$  and (c)  $b_f = 1.0$ . Relaxation time as a function of packing fraction for (b)  $b_f = 0.2$  and (d)  $b_f = 1.0$ .  $\nu_\parallel = 1.08$ ,  $\beta = 0.84$  and  $\nu_\perp = 0.59$  are Manna exponents in  $3d$ .

rather than reaching an evolving steady state like SGD. To sample multiple “active states” using GD one needs to generate multiple relaxations from random initial conditions.

#### Flatness of minima in the active phase of SGD.

We have shown that pairwise and particle-wise SGD behave similarly near the critical point (Figs. 5(b), 3 and Supplementary Material). Here, we explore their behavior above the critical point, examining the steady state energy susceptibility of the two processes. We perturb the steady state particle positions  $\mathbf{X}_T = [\mathbf{x}_T^1, \mathbf{x}_T^2, \dots, \mathbf{x}_T^N]$ , at time step  $k = T$ , by the Gaussian noise,  $\delta\mathbf{X} \sim \mathcal{N}(\mathbf{0}, \sigma^2 \mathbf{I})$ , and calculate the average energy fluctuations  $\Delta V = \langle V(\mathbf{X}_T + \delta\mathbf{X}) - V(\mathbf{X}_T) \rangle_{\delta\mathbf{X}}$ . Since  $\mathbf{X}_T$  is near a local minimum, higher  $\Delta V$  indicates greater susceptibility to positional perturbations.  $\Delta V$  also serves as a measure of the flatness of the minima, as illustrated in Fig. 4. If  $V$  is second-order smooth,  $\Delta V$  scales as the trace of the Hessian,  $\Delta V \propto \text{Tr}(H)$  (see Supplemental Material) which has been used to quantify the flatness of the loss landscape of DNNs [56].

We compare the two SGD schemes by perturbing the steady-state configuration with the same dimensionless noise variance,  $\tilde{\sigma} = \sigma/R$ , and calculate the dimensionless energy fluctuation  $\Delta\tilde{V} = \Delta V/U_0$  where  $U_0 \equiv U(r=0)$  measures the energy scale for the pairwise repulsion. Fig. 4 demonstrates that for particle-wise SGD, smaller batch sizes lead to sharper minima. Conversely, pairwise SGD is biased towards flatter minima for smaller batch sizes. This qualitative difference stems from their distinct stochastic dynamics. In particle-wise SGD, each particle’s displacement follows its local gradient to minimize the total potential energy  $V$ , with smaller batch sizes leading to less efficient gradient descent since only a subset of particle positions is updated. In contrast, at each step, pairwise SGD selects a subset of active pairs

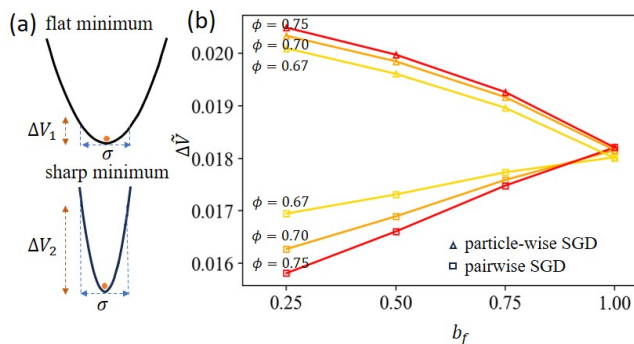


FIG. 4. Energy fluctuations of SGD steady state configurations under positional perturbations. (a) When the perturbation is of order  $\sigma$ , the energy fluctuation for the flat minimum ( $\Delta V_1$ ) is smaller than for the sharp minimum ( $\Delta V_2$ ). (b) Dimensionless energy fluctuation  $\Delta \tilde{V}$  as a function of batch fraction,  $b_f$ , for a number of packing fractions,  $\phi$ . For  $b_f = 1.0$ , SGD reduces to gradient descent. Each curve is averaged over 8 independent simulations, and each steady state configuration is perturbed 4000 times to measure  $\Delta \tilde{V}$  with  $\tilde{\sigma} = 0.03$ .

to define a random partial energy landscape,  $V'$ , which it minimizes. This process, similar to SGD in neural networks, favors flat minima [56–58]. Our findings suggest that using small batch sizes for the random construction of the partial energy landscape, as in pairwise SGD, is essential for finding flat minima. This cannot be achieved by following the gradient of the total energy, as done in particle-wise SGD.

**Discussion.** Our work demonstrates that displacement noise in BRO and selection noise in SGD play similar roles. Despite their different sources of randomness, all these processes converge to the same limiting packing fraction  $\phi_c \rightarrow 0.64$  as the kick size,  $\epsilon \rightarrow 0$  (or learning rate  $\alpha \rightarrow 0$  for SGD). Note that  $\phi_c \approx 0.64$  represents the upper limit on the maximum capacity achievable by SGD. Although denser packings exist – such as face-centered cubic packing ( $\phi_{FCC} = \pi/\sqrt{18} \approx 0.74$ ) [45, 59]) – these configurations are not found by SGD when starting from random initial conditions. Greater maximum capacity, could be achieved by tuning the initial conditions or by applying SGD to systems of polydisperse spheres [46] or ellipsoids [60], which more closely approximate neural manifolds. Near the critical point, the details of different noise protocols becomes negligible, with all schemes exhibiting behavior consistent with the Manna universality class (a property that we expect to hold for polydisperse spheres and ellipsoids). However, above the critical packing fraction,  $\phi > \phi_c$ , the nature of the random process used to construct the SGD gradients significantly affects the type of minima reached by the algorithm. Notably, only pairwise SGD exhibits a bias towards flat minima, reinforcing our analogy with loss minimization in neural networks.

This work paves the way for understanding how neu-

ral manifolds could evolve through a mechanism equivalent to SGD. Our results can be extended to higher dimensions, corresponding to classification problems in neural state space. We hypothesize that, as the number of classes (equivalent to the number of particles in our model) approaches infinity and the number of dimensions  $d \geq 4$ , the critical behavior of SGD will be in the mean-field universality class, given that the upper critical dimension for the Manna universality class is  $d = 4$  (a fact that was verified numerically for BRO [37]). Finally, our results offer a way of designing representation learning algorithms based on physical principles.

We particularly thank David J. Heeger for crucial comments on this work. We also thank Satyam Anand, Mathias Casiulis, Paul M. Chaikin, Dov Levine, Flaviano Morone, Aaron Shih and Sam Wilken for valuable discussions. This work was supported by the National Science Foundation grant IIS-2226387, National Institute of Health under award number R01EY035242, Simons Center for Computational Physical Chemistry, and in part by the NYU IT High Performance Computing resources, services, and staff expertise.

\* gz2241@nyu.edu

† sm7683@nyu.edu

- [1] S. Bubeck *et al.*, Foundations and Trends in Machine Learning **8**, 231 (2015).
- [2] C. M. Bishop and N. M. Nasrabadi, *Pattern recognition and machine learning*, Vol. 4 (Springer, 2006).
- [3] C. M. Bishop and H. Bishop, *Deep learning: foundations and concepts* (Springer, 2024).
- [4] Y. Bengio, in *Neural networks: Tricks of the trade: Second edition* (Springer, 2012) pp. 437–478.
- [5] D. E. Rumelhart, G. E. Hinton, and R. J. Williams, *nature* **323**, 533 (1986).
- [6] L. Bottou and Y. Cun, *Advances in neural information processing systems* **16** (2003).
- [7] Y. Bengio, in *Proceedings of ICML workshop on unsupervised and transfer learning* (JMLR Workshop and Conference Proceedings, 2012) pp. 17–36.
- [8] Q. Wang, Y. Ma, K. Zhao, and Y. Tian, *Annals of Data Science*, 1 (2020).
- [9] K. Janocha and W. M. Czarnecki, arXiv preprint arXiv:1702.05659 (2017).
- [10] M. Geiger, S. Spigler, S. d’Ascoli, L. Sagun, M. Baity-Jesi, G. Biroli, and M. Wyart, *Physical Review E* **100**, 012115 (2019).
- [11] F. Pellegrini and G. Biroli, *Advances in Neural Information Processing Systems* **33**, 5356 (2020).
- [12] A. Krizhevsky, I. Sutskever, and G. E. Hinton, *Advances in neural information processing systems* **25** (2012).
- [13] K. Simonyan and A. Zisserman, arXiv preprint arXiv:1409.1556 (2014).
- [14] A. Jacot, F. Gabriel, and C. Hongler, *Advances in neural information processing systems* **31** (2018).
- [15] C. Gerbelot, E. Troiani, F. Mignacco, F. Krzakala, and L. Zdeborova, *SIAM Journal on Mathematics of Data*

- Science **6**, 400 (2024).
- [16] Q. Li, C. Tai, and E. Weinan, in *International Conference on Machine Learning* (PMLR, 2017) pp. 2101–2110.
- [17] Q. Li, C. Tai, and E. Weinan, *The Journal of Machine Learning Research* **20**, 1474 (2019).
- [18] G. Rotskoff and E. Vanden-Eijnden, *Communications on Pure and Applied Mathematics* **75**, 1889 (2022).
- [19] N. Yang, C. Tang, and Y. Tu, *Physical Review Letters* **130**, 237101 (2023).
- [20] S. Mei, A. Montanari, and P.-M. Nguyen, *Proceedings of the National Academy of Sciences* **115**, E7665 (2018).
- [21] W. Azizian, F. Iutzeler, J. Malick, and P. Mertikopoulos, *arXiv preprint arXiv:2406.09241* (2024).
- [22] H. Li, Z. Xu, G. Taylor, C. Studer, and T. Goldstein, *Advances in neural information processing systems* **31** (2018).
- [23] S. K. Ainsworth, J. Hayase, and S. Srinivasa, *arXiv preprint arXiv:2209.04836* (2022).
- [24] T. Chen, S. Kornblith, M. Norouzi, and G. Hinton, in *International conference on machine learning* (PMLR, 2020) pp. 1597–1607.
- [25] K. He, H. Fan, Y. Wu, S. Xie, and R. Girshick, in *Proceedings of the IEEE/CVF conference on computer vision and pattern recognition* (2020) pp. 9729–9738.
- [26] P. Goyal, Q. Duval, I. Seessel, M. Caron, I. Misra, L. Sagun, A. Joulin, and P. Bojanowski, *arXiv preprint arXiv:2202.08360* (2022).
- [27] J. D. Bernal and J. Mason, *Nature* **188**, 910 (1960).
- [28] R. P. Behringer and B. Chakraborty, *Reports on Progress in Physics* **82**, 012601 (2018).
- [29] J. H. Conway and N. J. A. Sloane, *Sphere packings, lattices and groups*, Vol. 290 (Springer Science & Business Media, 2013).
- [30] S. Chung, D. D. Lee, and H. Sompolinsky, *Physical Review X* **8**, 031003 (2018).
- [31] S. Chung, D. D. Lee, and H. Sompolinsky, *Physical Review E* **93**, 060301 (2016).
- [32] F. Mignacco, C.-N. Chou, and S. Chung, *arXiv preprint arXiv:2405.06851* (2024).
- [33] L. Corte, P. M. Chaikin, J. P. Gollub, and D. J. Pine, *Nature Physics* **4**, 420 (2008).
- [34] S. Wilken, R. E. Guerra, D. J. Pine, and P. M. Chaikin, *Phys. Rev. Lett.* **125**, 148001 (2020).
- [35] E. Tjhung and L. Berthier, *Physical review letters* **114**, 148301 (2015).
- [36] S. Wilken, R. E. Guerra, D. Levine, and P. M. Chaikin, *Physical Review Letters* **127**, 038002 (2021).
- [37] S. Wilken, A. Z. Guo, D. Levine, and P. M. Chaikin, *Phys. Rev. Lett.* **131**, 238202 (2023).
- [38] L. Galliano, M. E. Cates, and L. Berthier, *Phys. Rev. Lett.* **131**, 047101 (2023).
- [39] D. Hexner and D. Levine, *Phys. Rev. Lett.* **118**, 020601 (2017).
- [40] F. Mignacco, F. Krzakala, P. Urbani, and L. Zdeborová, *Advances in Neural Information Processing Systems* **33**, 9540 (2020).
- [41] F. Mignacco and P. Urbani, *Journal of Statistical Mechanics: Theory and Experiment* **2022**, 083405 (2022).
- [42] R. D. Kamien and A. J. Liu, *Physical review letters* **99**, 155501 (2007).
- [43] A. Donev, F. H. Stillinger, and S. Torquato, *Physical review letters* **95**, 090604 (2005).
- [44] K. W. Desmond and E. R. Weeks, *Physical Review E* **80**, 051305 (2009).
- [45] A. Zaccone, *Phys. Rev. Lett.* **128**, 028002 (2022).
- [46] C. Anzivino, M. Casiulis, T. Zhang, A. S. Moussa, S. Martiniani, and A. Zaccone, *The Journal of Chemical Physics* **158** (2023).
- [47] C. Ness and M. E. Cates, *Physical review letters* **124**, 088004 (2020).
- [48] W. Hu, C. J. Li, L. Li, and J.-G. Liu, *Annals of Mathematical Sciences and Applications* **4** (2019).
- [49] M. Stephan, M. D. Hoffman, D. M. Blei, *et al.*, *Journal of Machine Learning Research* **18**, 1 (2017).
- [50] J. Lennard and I. Jones, *Proceedings of the Royal Society of London. Series A, containing papers of a mathematical and physical character* **106**, 441 (1924).
- [51] J. D. Weeks, D. Chandler, and H. C. Andersen, *The Journal of chemical physics* **54**, 5237 (1971).
- [52] S. Martiniani, P. M. Chaikin, and D. Levine, *Physical Review X* **9**, 011031 (2019).
- [53] E. Tjhung and L. Berthier, *Journal of Statistical Mechanics: Theory and Experiment* **2016**, 033501 (2016).
- [54] M. Henkel, H. Hinrichsen, and S. Lubeck, *Non-Equilibrium Phase Transitions*, 2009th ed., *Theoretical and mathematical physics* (Springer, New York, NY, 2009).
- [55] A. Sorge, *Zenodo: A scientific Python package for finite-size scaling analysis* (2015).
- [56] S. Jastrzębski, Z. Kenton, D. Arpit, N. Ballas, A. Fischer, Y. Bengio, and A. Storkey, *arXiv preprint arXiv:1711.04623* (2017).
- [57] Z. Xie, I. Sato, and M. Sugiyama, *arXiv preprint arXiv:2002.03495* (2020).
- [58] N. S. Keskar, D. Mudigere, J. Nocedal, M. Smelyanskiy, and P. T. P. Tang, *arXiv preprint arXiv:1609.04836* (2016).
- [59] T. C. Hales, *arXiv preprint math/9811071* (1998).
- [60] A. Donev, I. Cisse, D. Sachs, E. A. Variano, F. H. Stillinger, R. Connelly, S. Torquato, and P. M. Chaikin, *Science* **303**, 990 (2004).

## Appendix

**Stochastic approximation of particle-wise BRO.**  
In particle-wise BRO, the update rule for active particle  $i$  at iteration  $k$  reads,

$$\mathbf{x}_{k+1}^i = \mathbf{x}_k^i + u_k^i \sum_{j \in \Gamma^i} \Delta \mathbf{x}_k^{ji}. \quad (\text{A1})$$

where  $\Delta \mathbf{x}_k^{ji} = -\frac{\mathbf{x}_k^j - \mathbf{x}_k^i}{|\mathbf{x}_k^j - \mathbf{x}_k^i|} \cdot u_k^i$  is a particle-wise noise sample drawn uniformly from  $[0, \epsilon]$  at iteration  $k$ .

To derive a stochastic approximation, we follow the same procedure as for pairwise BRO, decomposing the biased random kick into its mean value  $\mathbf{g}_k^i = \mathbb{E}[u_k^i \sum_{j \in \Gamma^i} \Delta \mathbf{x}_k^{ji}] = \frac{1}{2} \sum_{j \in \Gamma_k^i} \Delta \mathbf{x}_k^{ji}$  and the fluctuation

around the mean  $\mathbf{z}_k^i = u_k^i \sum_{j \in \Gamma^i} \Delta \mathbf{x}_k^{ji} - \mathbf{g}_k^i$ . We then approximate the random fluctuation by the Gaussian random variable,  $\boldsymbol{\eta}_i \sim \mathcal{N}(\mathbf{0}, \boldsymbol{\Sigma}^i)$  with covariance,  $\boldsymbol{\Sigma}^i = \mathbb{E}[\mathbf{z}_k^i \mathbf{z}_k^{iT}] = \frac{1}{3} \mathbf{g}_k^i \mathbf{g}_k^{iT}$ . Therefore, we approximate Eq. A1 by

$$\mathbf{x}_{k+1}^i = \mathbf{x}_k^i + \epsilon(\mathbf{g}_k^i + \boldsymbol{\eta}_i). \quad (\text{A2})$$

By rewriting  $\mathbf{g}_k^i = -\nabla^i V$ , we obtain the stochastic approximation for the particle-wise BRO.

$$\mathbf{x}_{k+1}^i = \mathbf{x}_k^i - \epsilon \nabla^i V + \frac{\epsilon}{\sqrt{3}} \sqrt{\boldsymbol{\Omega}^i} \cdot \boldsymbol{\xi}_k^i, \quad (\text{A3})$$

where  $\boldsymbol{\Omega}^i = \nabla^i V \nabla^i V^T$

The corresponding stochastic differential equation is,

$$d\mathbf{x}^i(t) = -\frac{\epsilon}{\tau} \nabla^i V dt + \frac{\epsilon}{\sqrt{3\tau}} \sum_j \sqrt{\boldsymbol{\Omega}^i(t)} \cdot d\mathbf{W}^{ji}(t) \quad (\text{A4})$$

where  $\mathbf{x}^i(t)$  and  $\boldsymbol{\Omega}^i(t)$  are the continuous-time counterparts of the discrete-time variables in Eq. A3 and  $\tau$  is the time scale measuring the time elapsed between two discrete steps (see Supplemental Materials).

### Stochastic approximation of particle-wise SGD

The particle-wise SGD update rule for active particle  $i$  at timestep  $k$  is

$$\mathbf{x}_{k+1}^i = \mathbf{x}_k^i - \alpha \theta_k^i \nabla^i V, \quad (\text{A5})$$

where

$$\theta_k^i = \begin{cases} 1, & \text{if active particle } i \text{ is selected at iteration } k \\ 0, & \text{otherwise} \end{cases}$$

Each active particles share the same probability,  $b_f$ , to be selected for the batch update, therefor  $p(\theta_k^i = 1) = b_f$  and the mean value and the covariance of the gradient descent move are

$$\begin{aligned} \mathbb{E}[-\alpha \theta_k^i \nabla^i V] &= -\alpha b_f \nabla^i V \\ \text{Cov}[-\alpha \theta_k^i \nabla^i V] &= \alpha^2 (b_f - b_f^2) \nabla^i V \nabla^i V^T \end{aligned} \quad (\text{A6})$$

We approximate  $-\alpha \theta_k^i \nabla^i V$  as

$$-\alpha \theta_k^i \nabla^i V \approx -\alpha b_f \nabla^i V + \alpha \sqrt{b_f - b_f^2} \sqrt{\boldsymbol{\Omega}^i} \cdot \boldsymbol{\xi}_k^i \quad (\text{A7})$$

such that the mean and covariance of  $-\alpha \theta_k^i \nabla^i V$  and its approximation (Eq. A7) are equal. Thus, the stochastic approximation of Eq. A5 is

$$\mathbf{x}_{k+1}^i = \mathbf{x}_k^i - \alpha b_f \nabla^i V + \alpha \sqrt{b_f - b_f^2} \sqrt{\boldsymbol{\Omega}^i} \cdot \boldsymbol{\xi}_k^i \quad (\text{A8})$$

and the corresponding stochastic differential equation is

$$d\mathbf{x}^i(t) = -\frac{\alpha b_f}{\tau} \nabla^i V dt + \frac{\alpha}{\sqrt{\tau}} \sqrt{b_f - b_f^2} \sum_j \sqrt{\boldsymbol{\Omega}^i(t)} \cdot d\mathbf{W}^{ji}(t). \quad (\text{A9})$$

When  $\alpha = \epsilon/b_f$  and  $b_f = 3/4$ , the stochastic approximations of particle-wise BRO and SGD are equivalent.

**Stochastic approximation of pairwise SGD** The pairwise SGD dynamics of one active pairs of particles  $(i, j)$  at time  $k$  is

$$\begin{aligned} \mathbf{x}_{k+1}^i &= \mathbf{x}_k^i - \alpha \theta_k^{ij} \nabla_i U(|\mathbf{x}_k^i - \mathbf{x}_k^j|) \\ \mathbf{x}_{k+1}^j &= \mathbf{x}_k^j - \alpha \theta_k^{ij} \nabla_j U(|\mathbf{x}_k^i - \mathbf{x}_k^j|) \end{aligned} \quad (\text{A10})$$

where  $U(|\mathbf{x}_k^i - \mathbf{x}_k^j|) > 0$  only if  $|\mathbf{x}_k^i - \mathbf{x}_k^j| < 2R$ , with  $R$  the particles radius, and

$$\theta_k^{ij} = \begin{cases} 1, & \text{if active pair } (i, j) \text{ is selected at iteration } k \\ 0, & \text{otherwise} \end{cases}$$

The active pairs share the same probability,  $b_f$ , to be selected for the batch update, therefore,  $p(\theta_k^{ij} = 1) = b_f$ . Thus, the mean value and the covariance of the gradient descent move are

$$\begin{aligned} \mathbb{E}[-\alpha \theta_k^{ij} \nabla^i U(\mathbf{x}_k^i - \mathbf{x}_k^j)] &= -\alpha b_f \nabla^i U(\mathbf{x}_k^i - \mathbf{x}_k^j) \\ \text{Cov}[-\alpha \theta_k^{ij} \nabla^i U(\mathbf{x}_k^i - \mathbf{x}_k^j)] &= \alpha^2 (b_f - b_f^2) \nabla^i U^{ij} \nabla^i U^{ijT} \end{aligned} \quad (\text{A11})$$

In the same way as for particle-wise SGD, we obtain the mean and covariance of  $-\alpha \theta_k^{ij} \nabla^j U(\mathbf{x}_k^i - \mathbf{x}_k^j)$ , yielding the stochastic approximation of a single pairwise interaction

$$\begin{aligned} \mathbf{x}_{k+1}^i &= \mathbf{x}_k^i - \alpha b_f \nabla^i U^{ij} + \alpha \sqrt{b_f - b_f^2} \sqrt{\boldsymbol{\Lambda}^{ji}} \cdot \boldsymbol{\xi}_k^i \\ \mathbf{x}_{k+1}^j &= \mathbf{x}_k^j - \alpha b_f \nabla^j U^{ij} + \alpha \sqrt{b_f - b_f^2} \sqrt{\boldsymbol{\Lambda}^{ij}} \cdot \boldsymbol{\xi}_k^j \end{aligned} \quad (\text{A12})$$

where  $\boldsymbol{\Lambda}^{ji} = \nabla^i U^{ij} \nabla^i U^{ijT}$  and  $\boldsymbol{\Lambda}^{ij} = \nabla^j U^{ij} \nabla^j U^{ijT}$ . Since Eq. A10 is reciprocal, the center of mass is conserved,  $\mathbf{x}_{k+1}^i + \mathbf{x}_{k+1}^j = \mathbf{x}_k^i + \mathbf{x}_k^j$ , and we can reduce this system of equations to a single equation by imposing the reciprocity constraint,  $\boldsymbol{\xi}_k^{ij} = -\boldsymbol{\xi}_k^{ji}$  on the noise. Then, adding the contribution of all the active pairs that overlap with particle  $i$ , we arrive at the stochastic approximation of pairwise SGD,

$$\mathbf{x}_{k+1}^i = \mathbf{x}_k^i - \alpha b_f \nabla^i V + \alpha \sqrt{b_f - b_f^2} \sum_{j \in \Gamma_k^i} \sqrt{\boldsymbol{\Lambda}^{ji}} \cdot \boldsymbol{\xi}_k^i, \quad (\text{A13})$$

### Numerical comparison of BRO, SGD, and stochastic approximations.

We evolve the stochastic approximation given by Eq. 6, along with BRO and SGD, and compare their respective mean square displacements,  $\text{MSD}(k) = \langle \frac{1}{N} \sum_i |\mathbf{x}_k^i - \mathbf{x}_0^i|^2 \rangle$ , at time step  $k = 10^4$ , for different schemes starting from the same initial configuration (Fig. 5(a) and Supplementary Material). We find that the MSD agrees between schemes for small kick sizes, while the stochastic approximation becomes less accurate for larger kick sizes, as expected. In addition, we find that the structure factor for BRO and SGD schemes are consistent near the critical point (Fig. S2).

In BRO, the critical packing fraction,  $\phi_c$ , which separates the absorbing from the active phase, approaches

the random close packing fraction,  $\phi_{RCP} \approx 0.64$  in three-dimension as the kick size  $\epsilon \rightarrow 0$ . In Fig. 5(b) we show that all the dynamics converge to the same critical packing fraction,  $\phi_c \rightarrow \phi_{RCP}$  as  $\epsilon \rightarrow 0$  (or learning rate  $\alpha \rightarrow 0$  for SGD). This result implies that  $\phi_c(\epsilon \rightarrow 0)$  is independent of both the noise level (quantified by  $b_f$ ) and the reciprocity of the dynamics (whether pairwise or particle-wise). This suggests that the specific noise characteristics of different SGD schemes become less significant near the critical point.

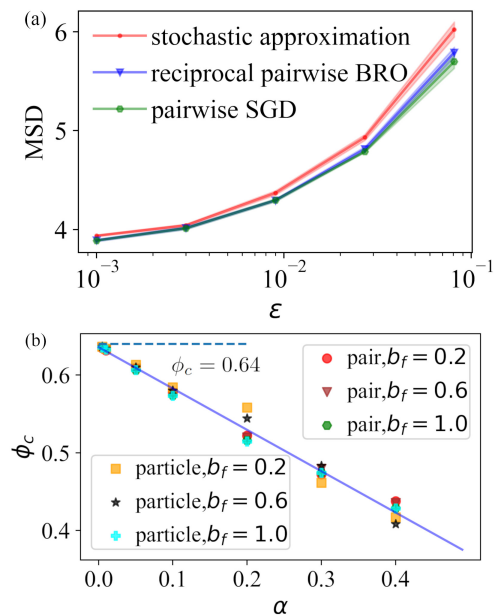


FIG. 5. (a) Mean square displacement (MSD) as a function of kick size ( $\epsilon$ ) for different schemes measured at time step,  $k = 10^4$ . For SGD schemes, we set  $\epsilon = 4\alpha/3, b_f = 3/4$  to match the BRO dynamics. (b) The critical packing fractions for pairwise and particle-wise SGD converge as  $\phi_c \rightarrow \phi_{RCP} \approx 0.64$  as  $\alpha \rightarrow 0$ . Both  $\alpha$  and  $\epsilon$  are measured in units of particle size,  $2R$ .